Generation and characterisation of an *Arabidopsis thaliana* *f3h*/*fls1*/*ans* triple mutant that accumulates eriodictyol derivatives

Hanna Marie Schilbert [1]* ORCID: 0000-0003-0474-7753

Mareike Busche [1]* ORCID: 0000-0002-2114-7613

Vania Sáez [2] ORCID: 0000-0002-6477-6671

Andrea Angeli [2] ORCID: 0009-0003-8882-5858

Bernd Weisshaar [1] ORCID: 0000-0002-7635-3473

Stefan Martens [2] ORCID: 0000-0001-9913-4882

Ralf Stracke [1#] ORCID: 0000-0002-9261-2279

[1] Bielefeld University, Faculty of Biology, Genetics and Genomics of Plants, 33615 Bielefeld, Germany

[2] Research and Innovation Centre, Fondazione Edmund Mach, San Michele all'Adige (TN), 38098, Italy

* These two authors contributed equally to this work.

[#] Corresponding author: ralf.stracke@uni-bielefeld.de

Abstract

Background: Flavonoids are plant specialised metabolites, which derive from phenylalanine and acetate metabolism. They possess a variety of beneficial characteristics for plants and humans. Several modification steps in the synthesis of tricyclic flavonoids cause for the amazing diversity of flavonoids in plants. The 2-oxoglutarate-dependent dioxygenases (2-ODDs) flavanone 3-hydroxylase (F3H, synonym FHT), flavonol synthase (FLS) and anthocyanidin synthase (ANS, synonym leucoanthocyanidin dioxigenase (LDOX)), catalyse oxidative modifications to the central C ring. They are highly similar and have been shown to catalyse, at least in part, each other's reactions. FLS and ANS have been identified as bifunctional enzymes in many species, including *Arabidopsis thaliana*, stressing the capability of plants to bypass missing or mutated reaction steps on the way to flavonoid production. However, little is known about such bypass reactions and the flavonoid composition of plants lacking all three central flavonoid 2-ODDs.

Results: To address this issue, we generated a *f3h*/*fls1*/*ans* mutant, as well as the corresponding double mutants and investigated the flavonoid composition of this mutant collection. The *f3h*/*fls1*/*ans* mutant was further characterised at the genomic level by analysis of a nanopore DNA sequencing generated genome sequence assembly and at the transcriptomic level by RNA-Seq analysis. The mutant collection established, including the novel double mutants *f3h*/*fls1* and *f3h*/*ans*, was used to validate and analyse the multifunctionalities of F3H, FLS1, and ANS *in planta*. Metabolite analyses revealed the accumulation of eriodictyol and additional glycosylated derivatives in mutants carrying the *f3h* mutant allele, resulting from the conversion of naringenin to eriodictyol by flavonoid 3'-hydroxylase (F3'H) activity.

Conclusions: We describe the *in planta* multifunctionality of the three central flavonoid 2-ODDs from *A. thaliana* and identify a bypass in the *f3h*/*fls1*/*ans* triple mutant that leads to the formation of eriodictyol derivatives. As (homo-)eriodictyol are known as bitter taste maskers, the annotated eriodictyol (derivatives) and in particular the knowledge gained about

their *in planta* production, could be used to genetically engineer the flavonoid composition of crops to improve the palatability of food produced from them.

Keywords: 2-oxoglutarate-dependent dioxygenases, enzyme promiscuity, flavonoid biosynthesis, flavonoids, multifunctionality, triple 2-ODD mutant

53 ## Background

54 Flavonoids are a large group of specialised metabolites with an estimated number of 9,000
55 flavonoid derivatives and a wide distribution throughout the plant kingdom (1). Flavonoids
56 share a basic structure with two aromatic C6 rings and a heterocyclic ring (2). Reorganisation
57 or modification, such as oxidation or glycosylation, is mainly responsible for the wide variety of
58 flavonoids. They can be classified into different subgroups including flavones, flavanones,
59 flavonols, dihydroflavonols, flavandiols, anthocyanins, and proanthocyanidins (2). These
60 subgroups exhibit manifold functions. Among others, anthocyanins promote pollination and
61 seed dispersal by colouring flowers and fruits (3-5), flavonols play a role in auxin transport,
62 plant fertility, and UV protection (6-8), and proanthocyanins serve as deterrent metabolites for
63 defence against bird predators (9). Moreover, flavonoids are beneficial for human nutrition due
64 to their antioxidative, antigenotoxic and anticarcinogenic properties (10, 11). These
65 health-promoting effects have led to a strong interest in increasing the flavonoid content in
66 plants (12, 13). However, as some flavonoids exhibit antinutritional properties, like a bitter-off
67 taste (14), the engineering of flavonoid composition is of high relevance for the breeding of
68 plants with desirable flavonoid profiles.

69 Flavonoid biosynthesis (Figure 1) is one of the best characterised pathways in plant specialised
70 metabolism. Due to the visible phenotypes of respective mutants which often display a
71 transparent testa resulting in yellow to pale-brown seed (15) and the large collections of
72 T-DNA- and transposon-tagged lines for *Arabidopsis thaliana* (16-18), the genes involved in
73 flavonoid biosynthesis are well studied. The flavonoid pathway is initiated by its key enzyme
74 chalcone synthase (CHS), which condensates *p*-coumaroyl-CoA and three molecules of
75 malonyl-CoA followed by cyclisation, leading to the formation of naringenin chalcone (19). A
76 heterocyclic ring is introduced spontaneously or through the catalysis of chalcone isomerase
77 (CHI), forming naringenin (20). Flavanone 3-hydroxylase (F3H or FHT) converts naringenin, a
78 flavanone, to dihydrokaempferol, a dihydroflavonol, by hydroxylation at the C-3 position (21).
79 In alternative branches, the flavonoid 3'-hydroxylase (F3'H) converts naringenin to eriodictyol
80 and dihydrokaempferol to dihydroquercetin (22). Naringenin can also be converted to flavones

81 by flavone synthaseI or II (FNSI or II) (23, 24). However, flavones were thought to be absent
82 in *A. thaliana* until two derivatives (7-2″,3″-diacetylglucoside and pentamethoxydihydroxy
83 flavone) were identified in Columbia-0 (Col-0) leaves (25, 26). DOWNY MILDEW
84 RESISTANT6 (*Ath*DMR6), a 2-oxoglutarate-dependent dioxygenase (2-ODD), has been
85 proposed as the enzyme responsible for their biosynthesis (26). The enzyme flavonol synthase
86 (FLS) uses dihydroflavonols to form flavonols by introducing a double bond between C-2 and
87 C-3 (27). Alternatively, dihydroflavonol 4-reductase (DFR) can reduce dihydroflavonols to the
88 corresponding leucoanthocyanidins, thus competing with FLS for substrates (28, 29).
89 Anthocyanidin synthase (ANS, also known as leucoanthocyanidin dioxygenase (LDOX))
90 converts leucoanthocyanidins to anthocyanidins (30). Anthocyanidins can be modified by
91 glycosyltransferases (GTs) to form anthocyanins, or they can be converted to
92 proanthocyanidins by anthocyanidin reductase (ANR) (31, 32). Besides anthocyanidins, other
93 flavonoids like flavonols or flavanones can be modified by GTs to form the respective
94 glycosides (33-35).
95 F3H, FNSI, FLS and ANS belong to the 2-ODD enzyme family (36). 2-ODDs represent the
96 second largest enzyme family in plants (37). They are ubiquitously spread across the plant
97 kingdom but also microorganisms and are involved in a variety of primary and specialised
98 metabolism, including the synthesis of specialised metabolites, hormones, signalling
99 molecules, amino acid modification and DNA-repair (summarised in 38, 39). Plant 2-ODDs can
100 be classified into three classes, DOXA, DOXB and DOXC, based on amino acid sequence
101 similarity, with DOXC harbouring 2-ODDs involved in the synthesis of specialised metabolites,
102 such as flavonoids, including F3H and FNSI (DOXC28) and FLS and ANS (DOXC47) (37).
103
104

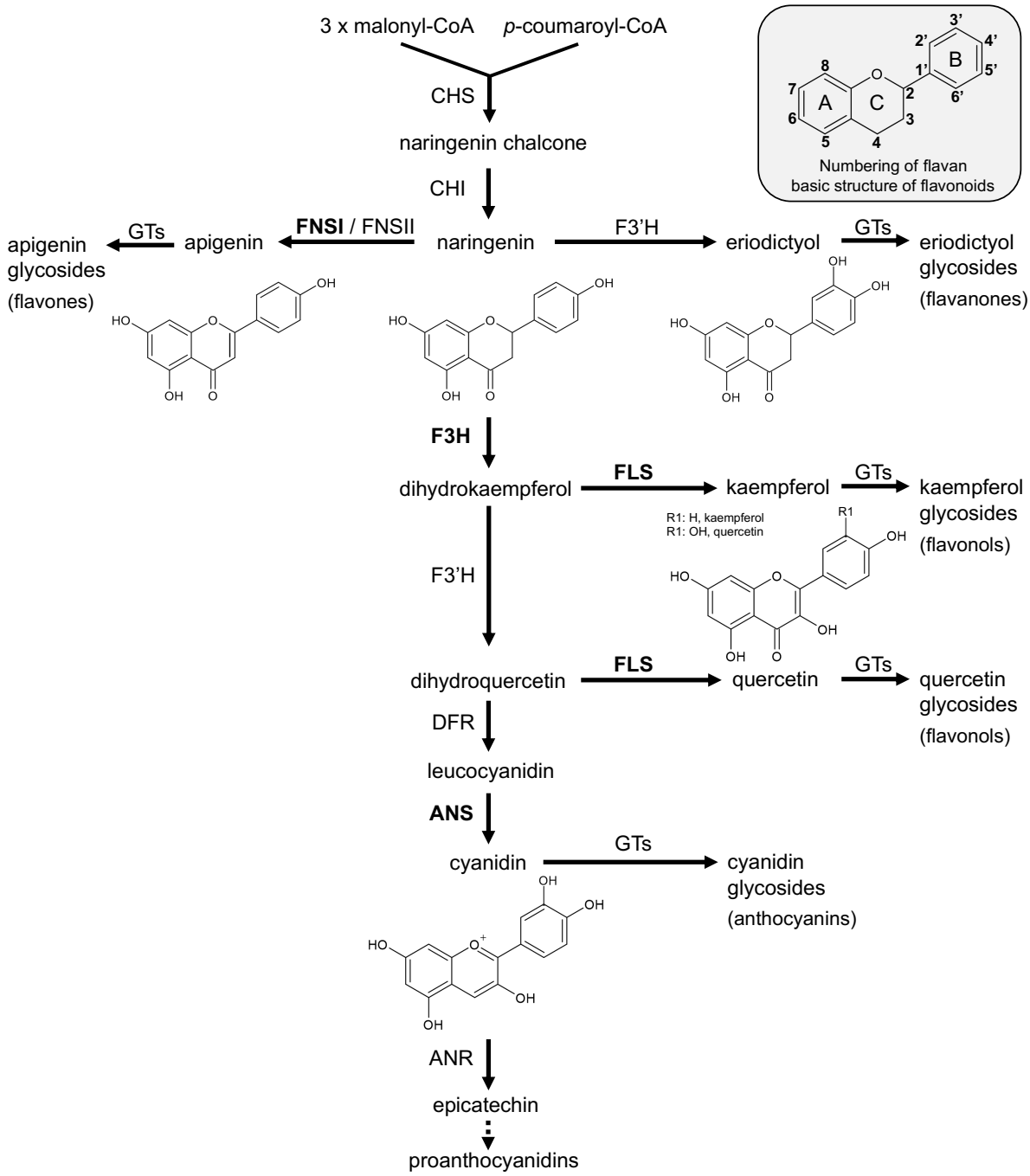

Figure 1: Simplified representation of the flavonoid biosynthesis pathway in plants. Details and abbreviations are given in the text. The 2-ODDs of the flavonoid biosynthesis F3H, FNSI, FLS, and ANS are shown in bold.

Characteristic hallmarks of 2-ODDs are generally (but not exclusively) the requirement of 2-oxoglutarate as co-reductant and iron as co-factor (36). Elucidation of the crystallographic structure of *Ath*ANS has identified the conserved amino acid residues involved in substrate-, co-factor-, and co-substrate binding (30). In addition, residues important for proper folding and substrate binding have been described (30).

116 As F3H, FLS and ANS all carry the conserved amino acid residues essential for 2-ODD activity,
117 it has been proposed that they share a common catalytic mechanism, possibly allowing
118 multifunctionality (40, 41). While FNSI and F3H often shows a narrow substrate spectrum (40,
119 42), FLS and ANS have been characterised as bi- or even multifunctional enzymes in several
120 species (40, 43-46). From an evolutionary perspective, it seems feasible that the oldest
121 enzyme, F3H, may have given rise to the other 2-ODDs involved in flavonoid biosynthesis
122 (summarised in 47) and that *Ath*FLS1 and *Ath*ANS retain *in vitro* F3H (40, 48) and, in the case
123 of *Ath*ANS, additional FLS side activity *in planta* (49). Due to the multifunctional nature of
124 flavonoid 2-ODD enzymes, comprehensive biochemical and functional characterisation is
125 required for unequivocal annotation, especially *in planta*. Only seven amino acid residues
126 distinguish parsley F3H from FNSI, providing an impressive example that amino acid
127 alignments are not sufficient for full functional characterisation (24).
128 The multifunctionalities of flavonoid 2-ODDs can be seen in the "leaky" phenotypes of *f3h*, *fls1*
129 and *ans* mutants of *A. thaliana* (21, 27, 49, 50), attributed to the partial compensation by other
130 2-ODDs. The *ans* mutant shows a significant reduction in anthocyanin and proanthocyanidin
131 content with almost unchanged flavonol levels compared to the wildtype (49, 51, 52), while the
132 *fls1* mutant shows a significant reduction in flavonol content and increased anthocyanin and
133 proanthocyanidin levels (49, 50, 53). The *f3h* mutant has a reduced flavonoid content, including
134 flavonols, anthocyanins, and proanthocyanidins, due to a generally reduced flux in the
135 flavonoid pathway (21, 54).
136 To unambiguously annotate the *in planta* multifunctionalities of F3H, FLS and ANS (which does
137 not necessarily reflect the *in vitro* function), multiple mutants are required, like it was done in
138 the case of the *fls1*/*ans* double mutant, which demonstrated the *in planta* FLS side activity of
139 ANS (40, 49).
140 In this study, we generated novel *A. thaliana f3h*/*fls1* and *f3h*/*ans* double mutants, as well as
141 an *f3h*/*fls1*/*ans* triple mutant to examine the phenotypic changes resulting from the loss of
142 activity of these flavonoid 2-ODDs. The *f3h*/*fls1*/*ans* mutant was characterised in detail, using
143 genomic, transcriptomic and metabolomic methods. Comprehensive phenotyping of the

144 flavonoid composition of the established flavonoid 2-ODD mutant set (composed of single,
145 double, and triple mutants) provided new insights into the *in planta* multifunctionalities of
146 *A. thaliana* F3H, FLS1 and ANS and the resulting metabolic fluxes. We found a flux into a
147 family of eriodictyol derivatives, which is most prominent in the *f3h*/*fls1*/*ans* triple mutant. The
148 knowledge gained in this study will be valuable for targeted engineering of flavonoid
149 composition and content in plants, especially crops.
150

151 # Results

152 ## Genomic characterisation of the *A. thaliana f3h*/*fls1*/*ans* mutant

153 To generate an *A. thaliana f3h*/*fls1*/*ans* mutant set, we used previously published insertional
154 alleles of the respective genes, showing the known loss-of-function phenotypes (*f3h* (*tt6-2*,
155 GK-292E08, Col-0 background), *fls1* (*fls1-2,* RIKEN_PST16145, Nö-0 background), *ans*
156 (*tds4-4*, SALK_073183, Col-0 background)). An *fls1*/*ans* double mutant was crossed with the
157 *f3h* single mutant. By screening the F2 progeny, homozygous *f3h*/*fls1*/*ans*, *f3h*/*fls1* and *f3h*/*ans*
158 mutants were identified by PCR-based genotyping. A *de novo* long-read assembly of the
159 *f3h*/*fls1*/*ans* mutant genome was generated to analyse the respective mutated loci at the
160 genomic level. The 160.57 Mbp assembly comprises 162 contigs with an N50 of 8.17 Mbp
161 (Supplementary Table S1). The assembly size slightly exceeds the size of the Col-0
162 Community-Consensus reference genome sequence assembly (133,336,906 bp) likely due to
163 the increased heterozygosity derived from the Nö-0 background of the *fls1* mutant. In total,
164 95.5 % complete BUSCOs were identified, indicating a high level of assembly completeness.
165 The assembly was used to validate the position of the T-DNA insertions at the *f3h* and *ans*
166 loci, and the position of the immobilised Ds transposon at the *fls1* locus (Figure 2). Two T-DNAs
167 comprising 11,393 bp sequence are inserted head-to-head into the 5'UTR of *f3h*, precisely
168 between 19,025,263 - 19,025,278 bp on chromosome three. The 5,417 bp Ds transposon is
169 inserted between 2,804,241 - 2,804,242 bp on chromosome five into the *fls1* locus in the first
170 exon. A large T-DNA array comprised of several T-DNAs and the corresponding binary vector

171 backbone (BVB) sequences was detected between 12,005,371 - 12,005,393 bp on
172 chromosome four, inserted into the front part of the second exon of *ans*. Due to the high amount
173 of repetitive sequences derived from this complex T-DNA array, the array is split across two
174 contigs in the assembly and therefore the exact size (spans >119 kbp) could not be
175 determined. A T-DNA left border (LB) was located at both ends of this insertion. Two additional
176 T-DNA insertion events have been identified (Supplementary Figure S1). However, these
177 insertions do not disrupt any additional annotated genes.

178

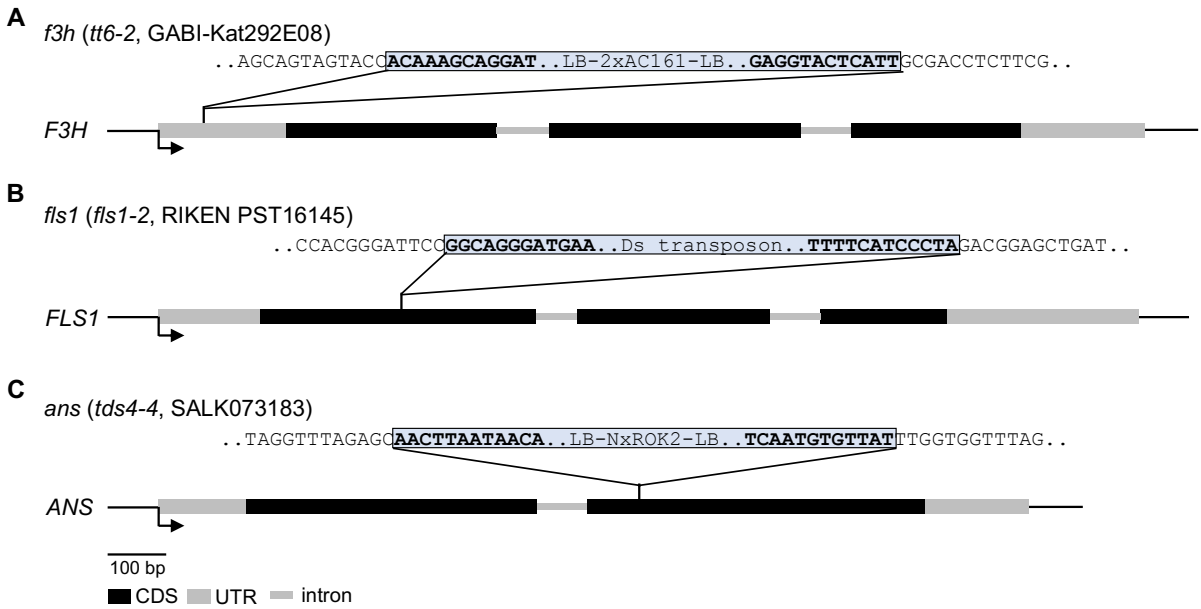

179

180 **Figure 2: Genomic characterisation of the *f3h*/*fls1*/*ans* mutant.** Schematic drawing of the
181 (A) *F3H* (*AT3G51240*), (B) *FLS1* (*AT5G08640*) and (C) *ANS* (*AT4G22880*) genes illustrating
182 the mutations in *f3h* (*tt6-2*), *fls1* (*fls1-2*) and *ans* (*tds4-4*), respectively. Black boxes mark the
183 CDSs and grey boxes indicate UTRs and grey thin lines indicate introns, bent arrows indicate
184 the transcription start. Dashed lines mark the respective T-DNA or transposon insertion.
185 Sequences belonging to the T-DNA or the transposon insertion are shown in a blue box in bold
186 and are flanked by the corresponding genomic sequences. LB, left border.
187

188 **Transcriptome analysis of the *f3h*/*fls1*/*ans* mutant**

189 To validate the insertion mutant alleles at the transcriptional level and to examine the
190 transcriptional changes that occur in the *f3h*/*fls1*/*ans* mutant, RNA-Seq data from six-days-old
191 seedlings were analysed. Col-0 and Nö-0 seedlings were used as controls. First, the
192 expression profiles of the respective knockout alleles were analysed in the *f3h*/*fls1*/*ans* mutant
193 (Supplementary Figure S2). For the *ans* and *fls1* mutant alleles, only marginal read coverage

194 was observed in the upstream regions of the T-DNA and transposon insertion positions,
195 respectively. These transcripts, which are greatly truncated compared to their normal lengths,
196 most likely result in non-functional proteins. Surprisingly, the *f3h* mutant allele showed a similar
197 expression profile as the wildtype allele, indicating that the *F3H* locus is still transcribed in the
198 *f3h*/*fls1*/*ans* mutant. However, mapping of the *f3h*/*fls1*/*ans* RNA-Seq reads to the *f3h*/*fls1*/*ans*
199 genome assembly revealed chimeric RNA-Seq reads containing the T-DNA LB sequence and
200 the sequence of the 5'UTR of *f3h*, emphasising that part of the T-DNA sequence is also
201 transcribed (Supplementary Figure S2). Several alternative translation start codons were
202 identified upstream of the original start site of *f3h* (Supplementary Figure S3), which could be
203 used for translation from the mutant *f3h* primary transcript and ultimately lead to a frameshift
204 and/or premature stop codon, resulting in a non-functional protein (refer to the discussion for
205 details).
206 In total, 1,643 and 1,203 differentially expressed genes (DEGs) were identified when
207 comparing *f3h*/*fls1*/*ans* with Col-0 and Nö-0, respectively (Figure 3, Supplementary File S1).
208 Of the DEGs derived from the comparison between *f3h*/*fls1*/*ans* and Col-0, 768 were
209 up-regulated and 875 were down-regulated, while 818 genes were up-regulated and 385
210 genes were down-regulated when *f3h*/*fls1*/*ans* was compared to Nö-0. To investigate the
211 transcriptional changes occurring in the *f3h*/*fls1*/*ans* mutant, 86 genes which are differentially
212 expressed between *f3h*/*fls1*/*ans* and Col-0 and between *f3h*/*fls1*/*ans* and Nö-0, but not
213 between Col-0 and Nö-0, were further analysed. After a manual screening (see Methods for
214 details), 35 DEGs remained, which are listed in Table 1. Of these, 28 were up-regulated in the
215 *f3h*/*fls1*/*ans* mutant. The *FLS1* gene was the only known gene related to flavonoid biosynthesis
216 in the list of DEGs.

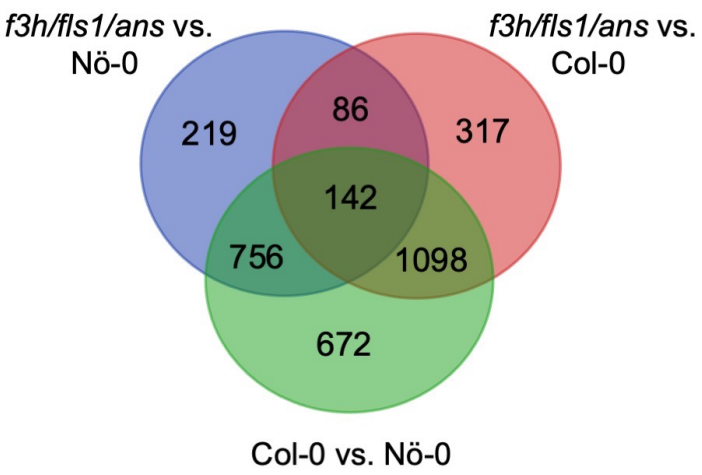

Figure 3: Venn diagram summarising the number of differentially expressed genes between seedlings of *f3h*/*fls1*/*ans* and the wildtypes Col-0 and Nö-0.

Table 1: List of differentially expressed genes in *f3h*/*fls1*/*ans* compared to Col-0 and Nö-0. AGI, Arabidopsis gene identifier; l2fc, $\log_2$ fold change; n.a., no annotation available.

AGI	l2fc vs. Col-0	l2fc vs. Nö-0	name / annotation
AT2G46765	7,25	5,74	hypothetical protein
AT5G08640	-5,54	-5,71	FLS1, flavonol synthase 1
AT2G20160	-4,71	-5,31	MEO, E3 ubiquitin ligase SCF complex subunit SKP1/ASK1 family protein
AT3G59884	3,35	1,84	MIR827A
AT2G14610	3,31	3,64	PR1 / CAPE9, pathogenesis-related protein 1
AT2G08820	2,3	1,37	n.a.
AT5G43570	2,22	1,38	PR-6 proteinase inhibitor family.
AT4G13493	2,21	1,64	MIR850A
AT4G06075	2,15	2,20	MIR5026 precursor
AT2G08825	2,11	1,40	n.a.
AT5G08855	2,11	1,96	n.a.
AT3G48560	2,08	2,14	AHAS / ALS, acetohydroxy acid synthase
AT3G46900	-1,98	-1,69	COPT2, Copper transporter 2, copper ion transmembrane transporter
AT1G52070	-1,93	-1,67	mannose-binding lectin superfamily protein
AT2G03850	1,93	1,07	LEA, late embryogenesis abundant protein family protein
AT2G11810	1,93	1,36	MGD3 / MGDC monogalactosyl diacylglycerol synthase 3
AT2G20723	1,84	1,79	snoRNA
AT2G20722	1,7	1,65	snoRNA
AT3G54730	1,62	3,16	transcription repressor
AT2G20670	1,52	1,62	DUF506, putative sugar phosphate exchanger
AT3G04210	1,36	1,59	TN13, disease resistance protein

AT2G44470	1,35	1,49	BGLU29, beta glucosidase 29
AT2G02850	1,34	1,16	ARPN, plantacyanin, copper ion binding
AT1G07135	1,29	1,23	glycine-rich protein
AT4G39675	1,28	1,32	hypothetical protein
AT1G60095	-1,27	-1,36	mannose-binding lectin superfamily protein
AT3G61930	1,26	1,17	hypothetical protein
AT2G07698	-1,23	-1,91	ATPase, F1 complex, alpha subunit protein
AT2G29330	1,23	1,54	TRI, tropinone reductase
AT1G36060	1,18	1,03	TG / WIND3, translucent green, Integrase-type DNA-binding superfamily protein
AT4G18980	1,18	1,58	AtS40-3
AT3G44260	1,17	1,13	CAF1A, Polynucleotidyl transferase, ribonuclease H-like superfamily protein
AT4G28420	1,14	1,62	tyrosine transaminase family protein
AT3G19430	-1,12	-1,90	LEA protein-like protein, late embryogenesis abundant protein-related
AT4G24570	1,01	1,10	DIC2, dicarboxylate carrier 2

224

225 **Phenotypic characterisation of the 2-ODD mutant collection including the novel**
226 ***f3h*/*fls1*, *f3h*/*ans*, and *f3h*/*fls1*/*ans* mutants**

227 To phenotypically characterise the flavonoid composition of the *f3h*/*fls1*/*ans* mutant compared
228 to the corresponding wildtypes, single and double mutants, the accumulation of flavanones,
229 flavonols, anthocyanins and proanthocyanidins (PA) was analysed (Figure 4, Figure 5). First,
230 the accumulation of flavonols was analysed in norflurazon-bleached seedlings, stained with
231 diphenylboric acid 2-aminoethyl ester (DPBA) (Figure 4A). Both wildtypes, Col-0 and Nö-0,
232 showed an orange colouration indicating the presence of quercetin glycosides. The *chs*
233 mutant, included as a control, is deficient in flavonol glycosides and thus appeared blue due
234 to sinapate derivatives. However, the *ans* mutant displayed an even more intense orange
235 fluorescence than the wildtypes. While the *f3h* mutant showed a red fluorescence, the *fls1*
236 mutant appeared green to light yellow. The *fls1*/*ans* mutant showed a pale yellow colour. The
237 novel *f3h*/*fls1*, *f3h*/*ans*, and *f3h*/*fls1*/*ans* mutants appeared red like the *f3h* mutant.
238 HPTLC and targeted UPLC-MS/MS analysis (including MRM quantification) of the flavonoid
239 composition in siliques revealed a wide range of flavonol glycosides in both wildtypes (Figure
240 4C, Supplementary Table S3). Consistent with DPBA staining, the *chs* mutant was deficient in
241 flavonoids. Accordingly, the level of *p*-coumaric acid was on average 186 µg per g dry weight

242 in *chs* siliques compared to up to 17 µg in all other lines, showing that this flavonoid precursor
243 accumulates in the *chs* mutant as the flavonoid biosynthesis pathway is blocked
244 (Supplementary Table S3). The *f3h*, *ans* and *f3h*/*ans* mutants showed a similar pattern of
245 flavonol glycosides as the wildtypes (Figure 4C). Moreover, the *ans* mutant accumulated the
246 highest amounts of flavonol glycosides with up to 3,549 µg quercetin-3-*O*-rhamnoside (Q-3R)
247 per g dry silique weight, whereas it was <273 µg in the other mutant lines and <2,656 µg in the
248 wildtypes (Supplementary Table S3). Accordingly, the *ans* knockout re-routes flavonoid
249 production to the flavonol biosynthesis branch while the other knockouts cause reduced
250 flavonol levels. The *fls1* mutant accumulated dihydroflavonols and small amounts of Q-3R,
251 whereas Q-3R levels decreased further to an average of 31.3 µg per g dry weight in *fls1*/*ans*
252 siliques while dihydroflavonol levels increased (Figure 4C and F, Supplementary Table S3).
253 The *fls1*/*ans* mutant accumulated the highest dihydroflavonol amounts compared to all lines
254 analysed, with an average dihydroquercetin level of 1,845 µg per g dry silique weight, showing
255 that dihydroflavonols accumulate when a further conversion to flavonols or anthocyanins is not
256 possible. Surprisingly, the *f3h*/*fls1* and *f3h*/*fls1*/*ans* mutants showed marginal and comparable
257 dihydroflavonols levels of up to 55 µg dihydrokaempferol per g dry weight, indicating the
258 presence of an (unknown) 2-ODD enzyme with F3H activity (Supplementary Table S3).
259 Interestingly, all mutant lines carrying the *f3h* allele accumulated a 'red (fluorescent)
260 metabolite', seen between Q-3R and K-3R-7R in HPTLC, indicating that a disruptive *f3h* allele
261 is essential for its production (Figure 4C). These results were in line with the red colouration of
262 *in situ* DPBA-stained seedlings carrying the *f3h* allele (Figure 4A). In contrast to flavonol
263 glycosides and dihydroflavonols, the accumulation of the 'red metabolite' was only visible late
264 after DPBA staining (Supplementary Figure S4). The accumulation of the 'red metabolite' was
265 further investigated in DPBA-stained siliques under white and UV light (Supplementary Figure
266 S5). The 'red metabolite' visibly accumulated in immature seeds (Figure 4B) of all lines carrying
267 the *f3h* knockout allele and was also observed under white light. The *f3h*/*ans* and *f3h*/*fls1*/*ans*
268 mutants showed the strongest intensity and the 'red metabolite' appeared to accumulate during
269 seed maturation (Supplementary Figure S5). In addition, it was detected in young stamens of

270 mutants harbouring the *f3h* allele (Supplementary Figure S6). Interestingly, the eriodictyol
271 content of all analysed lines measured by UPLC-MS/MS were similar to the accumulation
272 pattern of the 'red metabolite' observed by HPTLC (Figure 4C and E). In detail, the average
273 level of eriodictyol was <1.4 µg per g dry silique weight in lines with a functional *F3H* allele,
274 whereas the average eriodictyol content of *f3h* knockout lines increased to 170 µg in *f3h*,
275 300 µg in *f3h*/*fls1,* 457 µg in *f3h*/*ans* and 442 µg in *f3h*/*fls1*/*ans*, indicating that eriodictyol
276 accumulates as a consequence of the *f3h* knockout (Figure 4E). To further characterise the
277 'red metabolite', HPTLC was performed with available eriodictyol glycoside standards together
278 with methanolic extracts of Col-0 and *f3h*/*fls1*/*ans* siliques (Figure 4D). The 'red metabolite'
279 had the same retention factor (R_F) as eriodictyol-7-*O*-glucoside, while the R_F values of the
280 eriodictyol disaccharides and the eriodictyol aglycone differed from that of the 'red metabolite'.
281 Taken together, these results suggest that the metabolite underlying the red colouration of
282 mutants carrying the *f3h* allele is likely to be an eriodictyol hexoside, e.g.,
283 eriodictyol-7-*O*-glucoside.
284 Further chromatographic analysis with ion mobility separation in a high resolution mass
285 spectrometer (UPLC-TWIMS-QToF) on the *f3h*/*fls1*/*ans* flavonoid profile in siliques confirmed
286 the presence of eriodictyol-7-*O*-glucoside compared to a standard, the results show a mass
287 error below 3 ppm and an average of delta collision cross section (CCS) delta of 0.06 % in
288 ESI+ and 2.23 % in ESI- mode (Supplementary Table S4). The average content of
289 eriodictyol-7-*O*-glucoside determined by UPLC-MS/MS (High resolution mass spectrometry)
290 in the *f3h*/*fls1*/*ans* triple mutant is 10.38 µg per g dry weight (Supplementary Table S5).
291 Interestingly, the profile in *f3h*/*fls1*/*ans* is more complex (Supplementary Figures S7-S9). The
292 annotation of the eriodictyol derivates profile are based on $HDMS^E$ data, fragmentation
293 patterns by UPLC-MS/MS and isotopic distribution. The UPLC-TWIMS-QToF $HDMS^E$ profile
294 obtained in ESI+ and ESI- mode and subsequently UPLC-MS/MS analysis revealed the
295 presence of another eriodictyol hexoside, four di-hexosides, two tri-hexosides and two
296 rutinosides or neohesperidosides, respectively (Supplementary Tables S4 and S6). In ESI-
297 mode the main loss by UPLC-MS/MS is 162 Da (Supplementary Figure S9), corresponding to

298 the loss of a hexoside, the fragmentation has the presence of *m/z* 287, *m/z* 151 and *m/z*135
299 (Supplementary Figure S9), indicating a core with molecular formula $C_{15}H_{12}O_6$. Eriodictyol and
300 dihydrokaempferol have the same precursor, naringenin (Figure 1), and the same molecular
301 formula. Therefore, a comparison of fragmentation patterns, under the same methodology, of
302 eriodictyol and dihydrokaempferol standards by UPLC-MS/MS and UPLC-HDMS^E low and
303 high energy is required to improve the metabolite annotation. As is shown in Supplementary
304 Figures S10-S12, the absence of *m/z* 177 in all compounds of interest, including the
305 eriodictyol-7-*O*-glucoside, indicates an eriodictyol core. Two compounds, tentatively annotated
306 as eriodictyol rutinoside or neohesperidoside have two losses of 162 Da and 308 Da in
307 ESI- and 308 Da in ESI+ mode (Supplementary Figure S9, Supplementary Tables S4 and S6).
308 The presence of eriodictyol-7-*O*-rutinoside is excluded by the mismatch in retention time and
309 CCS values in the triple mutant by HDMS^e (Supplementary Table S4) and is in agreement with
310 the results shown in Figure 4D. Moreover, the dihydroquercetin profile of the *f3h*/*fls1*/*ans* triple
311 mutant compared to Col-0 is interesting, as it contains three different hexosides
312 (Supplementary Table S4). These results shed light on the accumulation of the eriodictyol and
313 dihydroquercetin aglycons and their subsequent modifications in the *f3h*/*fls1*/*ans* mutant.
314

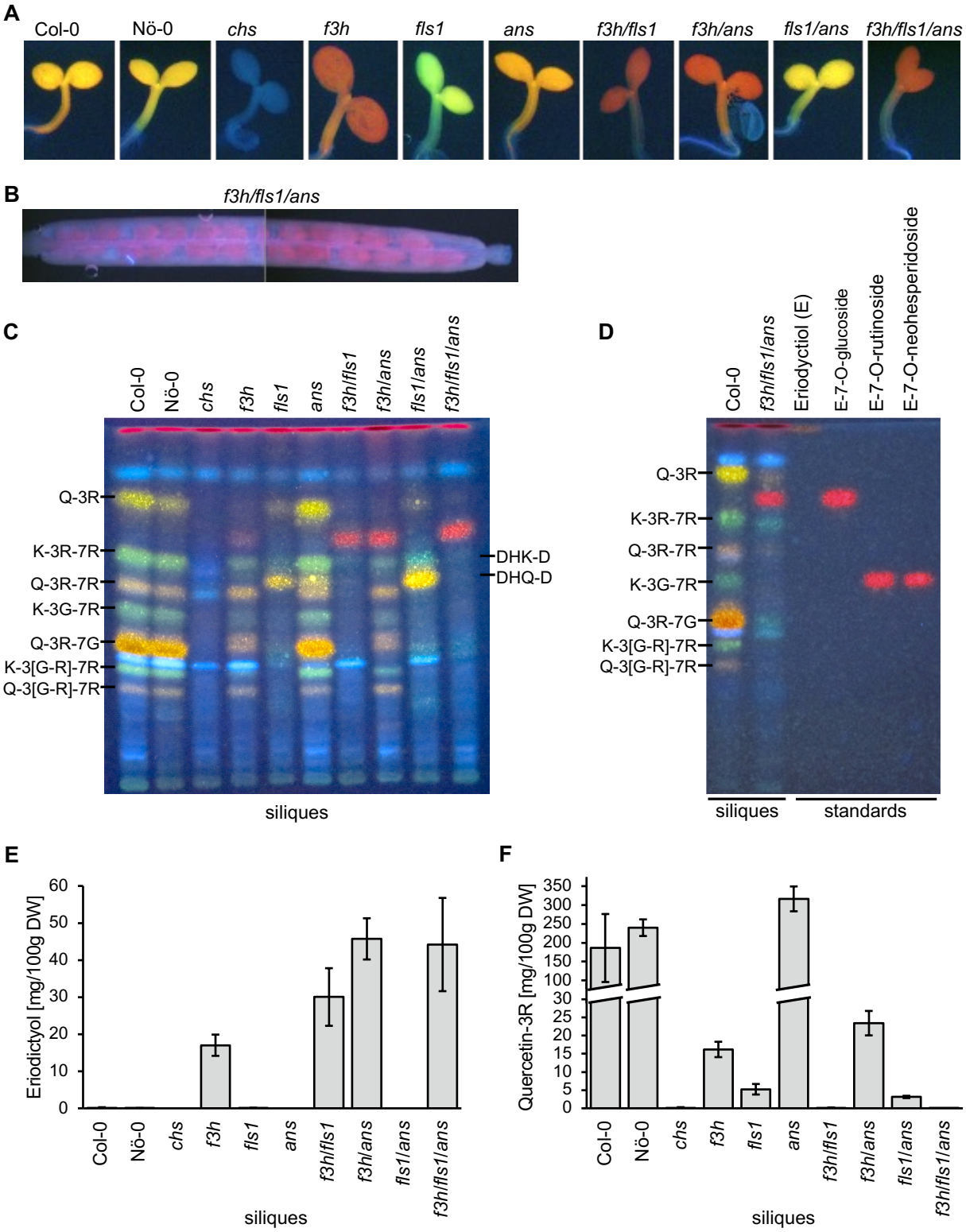

Figure 4: Accumulation of an eriodictyol hexoside in *A. thaliana* 2-ODD mutants carrying the *f3h* allele. (A) Seedlings stained *in situ* with diphenylboric acid 2-aminoethyl ester (DPBA) and visualised under UV light. Quercetin derivatives appear orange, kaempferol derivatives green, and blue corresponds to sinapate acid derivatives. (B) *In situ* DPBA-stained silique of the *f3h*/*fls1*/*ans* mutant visualised under UV light. (C) Accumulation of flavonol- and

322 dihydroflavonol glycosides in siliques analysed by HPTLC and visualised under UV light after
323 treatment with DPBA. Kaempferol derivatives are green, quercetin derivatives are orange and
324 sinapate acid derivatives are blue. G, glucose; K, kaempferol; Q, quercetin; R, rhamnose;
325 DHK-D, dihydrokaempferol derivative; and DHQ-D, dihydroquercetin derivative. (D) Eriodictyol
326 standards analysed by HPTLC and visualised under UV light after treatment with DPBA. E,
327 eriodictyol. (E) Eriodictyol and (F) quercetin-3-*O*-rhamnoside contents in siliques analysed by
328 UPLC-MS/MS MRM. Error bars indicate the standard deviation of four independent
329 measurements.

330

331 Besides flavanones and flavonols, other downstream (end-)products of the flavonoid
332 biosynthesis were analysed including anthocyanins and PAs. The accumulation of
333 anthocyanins was analysed in sucrose-induced, norflurazon-bleached seedlings (Figure 5A).
334 While both wildtypes, *f3h*, *fls1*, and *f3h*/*fls1* mutants show anthocyanin accumulation, *chs*, *ans*,
335 *f3h*/*ans*, *fls1*/*ans*, and *f3h*/*fls1*/*ans* mutants do not. These results are consistent with the
336 analysis in sucrose-induced, native seedlings and were validated by photometric quantification
337 of anthocyanins in seedlings (Figure 5A and B).
338 Seed pigmentation is influenced by the levels of PA in the seed coat, with a darker seed colour
339 corresponding to higher PAs levels. Analysis of the native seed colour of the wildtypes revealed
340 characteristic dark brown colour due to the presence of large amounts of PAs, while the *chs*
341 mutant showed a pale yellow seed indicative of the well-known PA deficiency and transparent
342 testa phenotype (Figure 5A). Most of the *2-ODD* mutants showed an intermediate seed colour
343 phenotype. However, the *fls1* mutant showed a similar brown seed colour as the wildtypes. In
344 accordance, UPLC-MS/MS analysis revealed that epicatechin levels of Col-0, Nö-0, and *fls1*
345 averaged between 799 µg and 1,108 µg per g dry silique weight, while all other lines showed
346 average levels <7 µg (Supplementary Table S3). Similar observations were made for
347 procyanidins (Figure 5D, Supplementary Table S3). Thus, PAs and their precursor epicatechin
348 are only produced in considerable amounts when *CHS, F3H*, and *ANS* are intact.

349

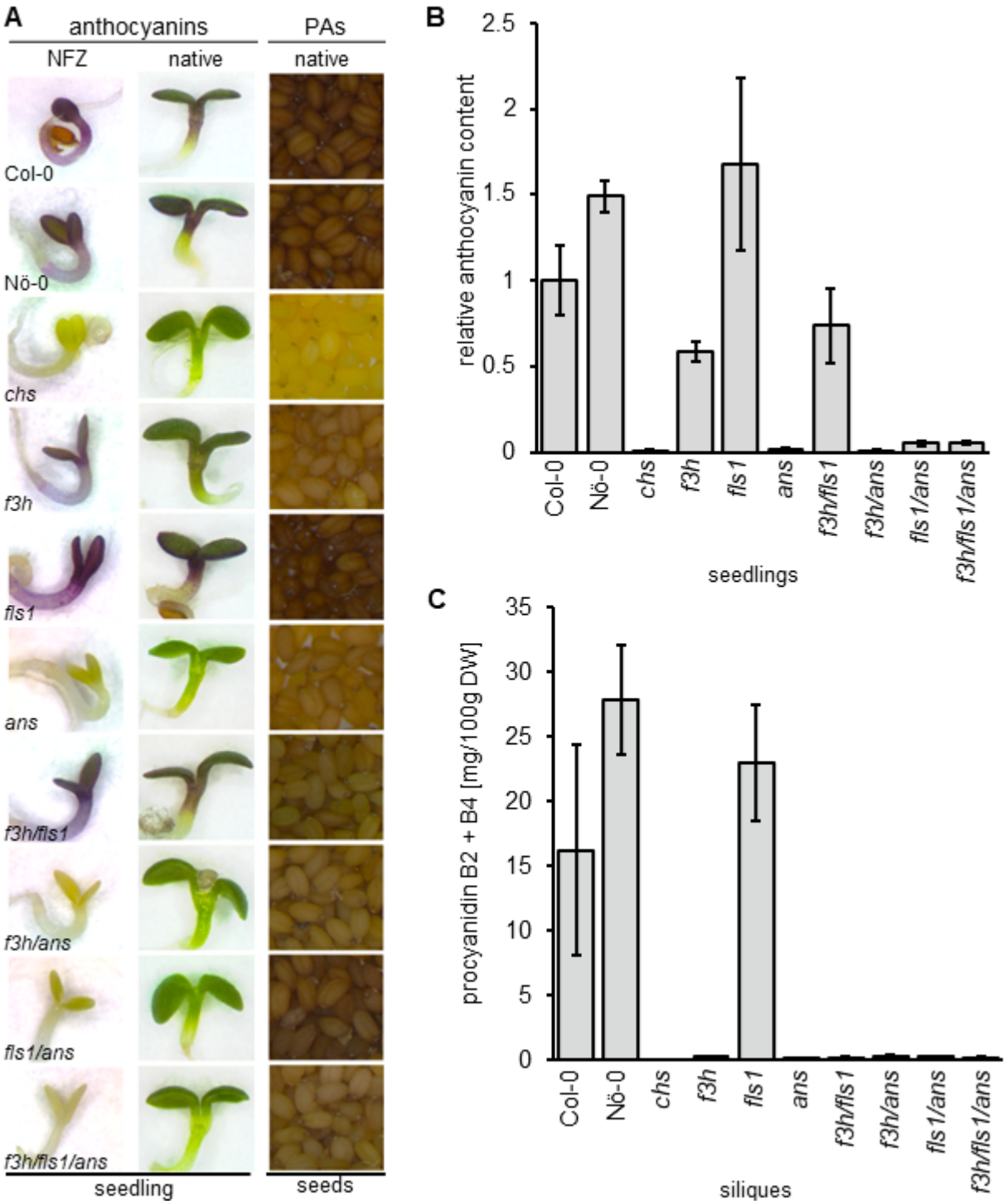

Figure 5: Anthocyanin and proanthocyanidin accumulation in *A. thaliana* 2-ODD mutants. (A) First column: norflurazon (NFZ)-bleached seedlings grown on 4% sucrose for anthocyanin induction. Second column: anthocyanin accumulation in seedlings grown on 0.5 MS plates with 4% sucrose. Third column: native seed colour. (B) Sucrose-induced anthocyanin accumulation in 6-days-old *A. thaliana* seedlings. Three independent biological replicates were measured for each sample. Error bars indicate standard deviation of the mean anthocyanin levels. (C) Procyanidin B2 + B4 content in siliques analysed by UPLC-MS/MS. Error bars indicate the standard deviation of four independent measurements.

360

361 ## Discussion

362 The three major flavonoid 2-ODD enzymes, F3H, FLS and ANS, are closely related and
363 therefore often have overlapping catalytic activities. We have generated an *A. thaliana*
364 *f3h*/*fls1*/*ans* mutant and analysed genomic, transcriptomic and phenotypic changes in order to
365 increase the knowledge about flavonoid biosynthesis related 2-ODDs in *A. thaliana.*

366 ### Genome sequence of the *f3h*/*fls1*/*ans* triple mutant

367 To characterise the *f3h*/*fls1*/*ans* triple mutant at the genomic level, a *de novo* Oxford Nanopore
368 Technology (ONT) genome assembly was generated. In-depth analysis of the respective
369 *2-ODD* mutant loci revealed the expected insertion positions per mutant allele (49, 51, 55). To
370 our knowledge, these mutant alleles have never been characterised using long-read
371 technology. Thus, in this study, the insertion of repeated T-DNAs and their BVB sequences at
372 the *ans* (*tds4-4*) locus were identified. Moreover, the ONT assembly revealed that two T-DNAs
373 inserted head-to-head in the 5'UTR of *f3h*. Such complex T-DNA insertion events, involving
374 arrays of multiple T-DNAs as well as BVB sequences, have been reported before to be more
375 the rule than the exception for *A. thaliana* T-DNA insertion mutants (56-59).

376 ### Transcriptome analysis of the *f3h*/*fls1*/*ans* triple mutant

377 RNA-Seq analysis in seedlings revealed that *FLS1* is the only differentially expressed *2-ODD*
378 between the *f3h*/*fls1*/*ans* mutant and the wildtypes. *ANS* and *F3H* were not identified as DEGs
379 due to remaining RNA-Seq read coverage at the *ans* and *f3h* loci upstream or downstream of
380 the T-DNA insertion site (Supplementary Figure S2). For *ANS*, which comprises two exons,
381 read coverage of the most of the first exon was observed upstream of the complex T-DNA
382 insertion array. The resulting transcript is severely truncated and, as previously confirmed by
383 the phenotype of the homozygous mutant (51, 52), results in a non-functional protein.

384

385 Interestingly, the expression level of the *f3h* locus was similar to that of the wildtype alleles and
386 covered the entire *F3H* exons. Comparison of the RNA-Seq data to the *f3h*/*fls1*/*ans* genome

387 assembly identified several chimeric RNA-Seq reads spanning part of the T-DNA and the
388 5'UTR of *f3h*, emphasising that part of the T-DNA::genome junction is transcribed.
389 Transcription is likely driven by the 2'promoter of the T-DNA, located 723 bp upstream of the
390 5'UTR of the *f3h* locus (Supplementary Figure S3). A similar observation was made in a
391 *phytochrome C* mutant by *Monte et al.* (60). They analysed a T-DNA insertion line that showed
392 *PHYC* transcript levels similar to the wildtype. However, protein analysis revealed, that the
393 plants did not accumulate the corresponding protein. Similar limitations are conceivable in our
394 study. The 11,393 bp T-DNA insertion could either lead to an extended and, in consequence,
395 non-functional protein or one of the start codons located on the T-DNA could be used as an
396 alternative start codon, ultimately resulting in a frameshift and/or premature stop codon
397 (Supplementary Figure S3). Taken together, the omics data and the very distinct phenotype of
398 the *f3h*/*fls1*/*ans* mutant strongly suggest a non-functional *f3h* allele, in line with previous results
399 (17, 55). Furthermore, genomic and transcriptomic data of the *ans* and *fls1* loci showed that
400 these loci are *null*-alleles.
401 Apart from the *FLS1* gene, no other genes encoding enzymes, regulators or transporters of
402 flavonoid biosynthesis were identified as DEGs between the *f3h*/*fls1*/*ans* mutant and the
403 wildtypes. Nevertheless, several identified DEGs are noteworthy. For example, *miR827A* is
404 upregulated in *f3h*/*fls1*/*ans*, compared to the wildtypes. *miR827* expression is known to be
405 sucrose-induced and it targets ethylene response factors (ERFs) to regulate the expression of
406 *SUCROSE SYNTHASE* which has been proposed as a regulator of anthocyanin biosynthetic
407 genes (61). Accordingly, increased *miR827A* expression could be a means of the *f3h*/*fls1*/*ans*
408 mutant to counteract anthocyanin deficiency. Of course, this requires an unknown feedback
409 regulation circuit. *TROPINONE REDUCTASE* (*TRI*) transcript abundance is increased in
410 *f3h*/*fls1*/*ans.* TRI has previously been reported to reduce the flavanone backbone (62). Since
411 the flavonol- and anthocyanin branches of flavonoid biosynthesis are blocked in the
412 *f3h*/*fls1*/*ans* mutant, flavanones like eriodictyol accumulate in *f3h*/*fls1*/*ans* and could be
413 reduced by TRI activity. *BETA GLUCOSIDASE29* (*BGLU29*) is upregulated in *f3h*/*fls1*/*ans*
414 compared to the wildtypes. BGLU29 belongs to the family of beta-glucosidase enzymes (63).

415 Although some BGLUs have been shown to be functional glucosyltransferases involved in the
416 glycosylation of flavonoids (BGLU10 (64) and BGLU6 (65)), it is very unlikely that BGLU29 has
417 glycosyltransferase activity, as it is most closely related to BGLU28 - BGLU32, all of which
418 having glycoside hydrolase activity (66). BGLU29 may be involved in the hydrolysis of flavonoid
419 glycosides. In addition, the expression of *ACETOHYDROXY ACID SYNTHASE* (*AHAS*), which
420 is involved in the biosynthesis of valine, leucine and isoleucine from pyruvate (67), is increased
421 in the *f3h*/*fls1*/*ans* mutant. Since flavonoids are derived from phenylalanine, increased *AHAS*
422 expression could hint to an accumulation of phenylalanine in *f3h*/*fls1*/*ans* and an effort by the
423 plant to produce other amino acids instead.

424 **Phenotype**

425 ***In planta* multifunctionality of flavonoid 2-ODDs**

426 Previous studies revealed a "leaky" phenotype of the *2-ODD* single mutants and the *fls1*/*ans*
427 double mutant, which was attributed to partial compensation of other 2-ODD dioxygenases,
428 e.g., the bi- and multifunctionality of FLS and ANS, respectively (21, 27, 49). Owens *et al.* (27)
429 showed, that FLS1 not only accepts dihydroflavonols as substrate, but can also convert
430 naringenin to dihydrokaempferol *in planta*, thus exhibiting F3H side activity. ANS has been
431 shown to produce dihydroquercetin and quercetin from naringenin *in vitro*, indicating its F3H
432 and FLS side activity (40, 68, 69). Furthermore, the accumulation of flavonol glycosides in the
433 *fls1* mutant and further flavonol reduction in the *fls1*/*ans* mutant showed that ANS also has an
434 FLS activity *in planta* (49). This knowledge is consistent with our analyses and the novel
435 *f3h*/*ans*, *f3h*/*fls1* and *f3h*/*fls1*/*ans* mutants allowed an in-depth analysis of the *in planta*
436 multifunctionality of F3H, FLS, and ANS. The flavonol glycoside patterns of the *f3h*, *ans* and
437 the novel *f3h*/*ans* mutants were like the ones of the wildtypes confirming the significant *in*
438 *planta* F3H activity of FLS1.

439 The *fls1*/*ans* mutant still accumulates flavonol glycosides, suggesting that F3H has additional
440 *in planta* FLS activity. Alternatively, FLS3 may have residual *in planta* FLS activity, as FLS *in*
441 *vivo* activity of FLS3 has been shown in yeast (70). As all mutant lines with a non-functional

442 ANS contain no anthocyanins, F3H and FLS do not seem to have any ANS activity. Finally,
443 the marginal and comparable amounts of dihydroflavonol of up to 55 µg dihydrokaempferol per
444 g dry silique weight identified in the *f3h*/*fls1* and *f3h*/*fls1*/*ans* mutants indicate that ANS does
445 not appear to have significant F3H activity *in planta*. However, the identification of residual
446 dihydroflavonols in the *f3h*/*fls1*/*ans* mutant was rather surprising since the two major flavonoid
447 2-ODD responsible for dihydroflavonol accumulation, F3H and FLS1, were knocked-out in this
448 mutant.
449 Although the biological significance of these trace amounts of dihydroflavonols and the
450 enzyme(s) leading to their production is questionable, it raises the question of which enzyme(s)
451 could be involved in their biosynthesis. The dihydroflavonols could be produced by an
452 (unknown) 2-ODD with F3H activity or F3H side activities of one of the FLS paralogs. While
453 *AthFLS2*, *AthFLS4*, *AthFLS5* and *AthFLS6* were identified as pseudogenes or encoding
454 non-functional proteins, minor FLS activity of *Ath*FLS3 was reported under prolonged assay
455 conditions in yeast (27, 70). Although FLS3 showed no F3H or FLS activity in *Escherichia coli*,
456 *in planta* F3H activity was identified for FLS3 homologs from banana and rapeseed, the latter
457 sharing 67 % amino acid sequence identity with *Ath*FLS3 (42, 46). To investigate a potential
458 *in planta* F3H and FLS activity of *Ath*FLS3, an *fls3* knockout allele could be introduced in the
459 *f3h*/*fls1*/*ans* mutant to generate a *fls3*/*f3h*/*fls1*/*ans* mutant. A reduction of dihydroflavonols and
460 flavonols in the *fls3*/*f3h*/*fls1*/*ans* mutant compared to the *f3h*/*fls1*/*ans* mutant would provide
461 evidence for an F3H and FLS activity of FLS3 *in planta*.
462 Alternatively, the production of residual dihydroflavonols in the *f3h*/*fls1*/*ans* mutant may involve
463 FNSI, another flavonoid 2-ODD closely related to F3H. Bifunctional enzymes with FNSI and
464 F3H activity have been identified in gymnosperms and mosses (71). FNSI enzymes were
465 thought to be restricted to the Apiaceae family (72) and thus absent from *A. thaliana,* until the
466 identification of a DOWNY MILDEW RESISTANT6 (DMR6/FNSI) homolog with FNSI activity,
467 alongside reports of functional FNSIs from liverworts, *Oryza sativa*, and *Zea mays* (26, 71, 73,
468 74). However, *DMR6*/*FNSI* is primarily expressed in leaves and not in siliques (26), where the
469 residual amounts of dihydroflavonols were detected. Moreover, the endogenous activity of

470 DMR6/FNSI is not sufficient to compensate the dihydroflavonol deficient phenotype of the
471 *f3h*/*fls1* or *f3h*/*fls1*/*ans* mutants, indicating that DMR6/FNSI does not have substantial F3H
472 activity *in planta*. Taken together, these findings suggest that if DMR6/FNSI harbours F3H side
473 activity, it is likely to play a minor role, if any, in the production of the residual dihydroflavonols
474 detected in *f3h*/*fls1*/*ans* siliques.
475 In summary, the established 2-ODD mutant collection could be used in the future to analyse
476 not only potential multifunctionality of DMR6/FNSI, but rather 2-ODDs in general. This is of
477 particular importance for the FNSI family, as it is no longer confined to the Apiaceae family,
478 and knowledge on FNSI multifunctionality is rare, especially in angiosperms (71, 75). As
479 mentioned above, flavonoid 2-ODDs show broad substrate specificities *in vitro,* which do not
480 necessarily correspond to product accumulation *in vivo* (21). This emphasises the importance
481 of the established mutant collection for the *in planta* characterisation of flavonoid 2-ODD
482 multifunctionality, especially for studies characterising their functionalities solely *in vitro* (76,
483 77). For example, *in planta* complementation experiments using the novel mutant collection
484 could validate the FLS side activity found *in vitro* and the absence of F3H side activity of
485 *Vitis vinifera*'s ANS (77).

486 **Flavonoid accumulation in the absence of the three major flavonoid 2-ODDs**

487 The mutant collection was harnessed to investigate changes in the metabolic flux associated
488 with the knockout of the three major flavonoid 2-ODDs F3H, FLS1, and ANS. Interestingly, all
489 mutant lines carrying the *f3h* allele accumulate a metabolite in seedlings, immature seeds,
490 young stamens and siliques, which appears 'red' after DPBA-staining in visible light and under
491 UV light. This 'red (fluorescent) metabolite' is absent in the wildtypes and is most clearly seen
492 in an HPTLC of methanolic extracts from siliques (Figure 4B). The characteristic red
493 fluorescence of the *f3h* seedlings after DPBA staining has previously been observed and
494 suggested to be derived from an orthodihydroxy- or orthotrihydroxy flavonoid (78). In addition,
495 3'hydroxylation of the B ring was suggested to be required for the red fluorescence upon
496 staining, as DPBA-stained *f3h*/*f3'h* and *chs*/*f3h* mutants showed a light blue to pale
497 fluorescence (78). Owens *et al.* (21) suggested that F3'H might convert the accumulating

498 naringenin to eriodictyol which could be further reduced to a 3-desoxy flavonoid by the FNR
499 activity of native DFR (21). We show that high levels of eriodictyol accumulate in siliques of
500 lines carrying an *f3h* knockout allele. This is in accordance with the high expression of *F3'H* in
501 siliques compared to flowers, leaves, stems, and roots (22). While HPTLC-based flavonoid
502 glycoside analysis showed that the 'red metabolite' is most likely an eriodictyol hexoside, the
503 results by UPLC-MS/MS and UPLC-TWIMS-QToF analyses revealed a profile with various
504 metabolites annotated as eriodictyol hexosides, including eriodictyol-7-*O*-glucoside, and
505 additional possible eriodictyols with neohesperidoside or rutinoside derivatisation.
506 We therefore postulate that F3'H converts naringenin to eriodictyol, which may then be further
507 modified by glycosylation via glycosyltransferases. For example, the
508 flavonoid-7-*O*-glycosyltransferase UGT73B1 has been shown to use eriodictyol as a preferred
509 substrate for the catalysis to eriodictyol-7-*O*-glycoside (35). Considering the previously
510 presented DEGs, the tropinone reductase (TRI) may be involved in eriodictyol reduction, as a
511 previous study showed that TRI can reduce flavanones *in vitro* (79). In the future, knockout
512 alleles of the identified candidate genes could be introduced in the *f3h*/*fls1*/*ans* mutant to
513 analyse their role in the eriodictyol hexoside biosynthesis and degradation.
514

515 ## Conclusions

516 We present a detailed characterisation of a novel *A. thaliana f3h*/*fls1*/*ans* mutant and the
517 corresponding single and double mutants. We have used genomic, transcriptomic, and
518 metabolite data to extend the knowledge about flavonoid 2-ODDs in *A. thaliana.* The set of *f3h,*
519 *fls1* and *ans* single, double and triple mutants will enable further work on flavonoid 2-ODDs
520 and their multifunctionalities in *A. thaliana*, as these are often limited to *in vitro* studies or
521 enzyme assays in *E. coli* or yeast (45, 76, 80). The *f3h*/*fls1*/*ans* mutant will also facilitate the
522 characterisation of multifunctional 2-ODDs from other species *in planta*. Finally, we have
523 shown that eriodictyol and several eriodictyol derivatives accumulate in the absence of a
524 functional F3H *in planta* with eriodictyol-7-*O*-glucoside being one of the predominant eriodictyol
525 derivatives. (Homo-)eriodictyols are bitter-masking flavanones with no additional strong taste

526 or flavour and are thus promising flavour modifiers for food applications and pharmaceuticals
527 (81). The knowledge gained from the production of eriodictyol (derivatives) could therefore be
528 used to genetically engineer the flavonoid composition of crops to improve the palatability of
529 derived food products.
530

531 # Methods

532 ## Plant material

533 Columbia-0 (Col-0, NASC ID N1092) and Nössen-0 (Nö-0, NASC ID N3081) accessions were
534 used as wildtype controls. A *chs* mutant (*tt4-11*, SALK_020583, Col-0 background, T-DNA
535 from pROK2 plasmid (18, 82)) was used as a flavonoid deficient control. The *A. thaliana*
536 mutants *f3h* (*tt6-2*, GK-292E08, Col-0 background, T-DNA from pAC161 plasmid (17)), *fls1*
537 (*fls1-2,* RIKEN_PST16145, Nö-0 background, Ds transposon (49);(16)), *ans* (*tds4-4*,
538 SALK_073183, Col-0 background (51, 52)) and an *fls1*/*ans* double mutant (49) were used for
539 crosses and as controls.

540 ## Crossing and genotyping of mutants

541 To generate the novel *f3h*/*fls1*, *f3h*/*ans*, and *f3h*/*fls1*/*ans* mutants, the *fls1*/*ans* double mutant
542 was crossed with the *f3h* mutant. Individuals of the F2 progeny were analysed by PCR
543 genotyping using GoTaq2 DNA polymerase (Promega) according to standard protocols.
544 Sequences of primers used for genotyping are provided in Supplementary Table S2. Plants
545 homozygous for the respective mutant alleles were used for further analyses.

546 ## DNA extraction, library construction, and sequencing

547 ONT was used to generate long-reads of the *f3h*/*fls1*/*ans* mutant. Genomic DNA was isolated
548 from rosette leaves using the NucleoBond HMW DNA Kit (Macherey-Nagel, Düren, Germany)
549 according to the manufacturer's instructions. DNA quality was assessed via PicoGreen
550 (Quant-iT) measurement on a FLUOstar OPTIMA plate reader (BMG labtech), and pulsed-field
551 gel electrophoresis. The Short Read Eliminator (SRE) Kit (Circulomics, Baltimore, MD, USA)

552 was used to enrich long DNA fragments and results were validated by PicoGreen
553 measurements. 1.2 µg of high molecular weight DNA was used for library preparation
554 according to the SQK-LSK109 protocol (Oxford Nanopore Technologies (ONT), Oxford, UK).
555 Sequencing was performed on a R9.4.1 flow cell on a GridION. The flow cell was treated with
556 nuclease flush to load another library twice. Basecalling was performed using Guppy v.4.2.3
557 (https://community.nanoporetech.com).

558 ***De novo* ONT genome assembly and read mapping**

559 A *de novo* ONT genome assembly of the *f3h*/*fls1*/*ans* mutant was constructed with Canu v2.1.1
560 (83). No polishing of the assembly was performed, as the assembly was only used to analyse
561 the respective mutant loci. Contigs <100 kb were removed, followed by the calculation of
562 assembly statistics as previously described (84). Assembly quality was assessed via BUSCO
563 v3.0.2 using the embryophyta_odb9 lineage dataset (85). For manual curation of loci of interest
564 reads were mapped to the *A. thaliana* TAIR10 reference genome sequence (86) using
565 minimap2 (87). Minimap2 was run in ONT mode (-ax map-ont) and no secondary alignments
566 were allowed (--secondary=no). BAM files were sorted and indexed using samtools (88).
567 Manual curation of regions of interest was performed by using Integrative Genomics Viewer
568 (89) and BLAST (90). The assembly data was screened for the presence of additional T-DNAs
569 using loreta (57).

570 **RNA-Seq analysis: Ribonucleic acid extraction, library construction, and**
571 **sequencing**

572 RNA was isolated from 6-days-old seedlings using the NucleoSpin® RNA Plant Kit
573 (Macherey-Nagel, Düren, Germany) according to the manufacturer's instructions. Four
574 biological replicates were used for each genotype (Col-0, Nö-0, and *f3h*/*fls1*/*ans*). The RNA
575 quality was validated using a 2100 Bioanalyzer system (Agilent, Santa Clara, CA, USA).
576 Sequencing libraries were constructed from 1 µg of total RNA, following the TrueSeq v2
577 protocol. Single end sequencing of 84 nt was performed on an Illumina NextSeq500 at the
578 Sequencing Core Facility of the Center for Biotechnology (CeBiTec) at Bielefeld University.

579 **RNA-Seq mapping and count table generation**

580 After assessing read quality using FastQC (91), reads were mapped to the *A. thaliana* Col-0
581 TAIR10 reference genome sequence (92) using STAR v.2.7.1a (93). STAR was run in Basic
582 mode allowing a maximum of 5 % mismatches per read length and using a minimum of 90 %
583 matches per read length. Mapping statistics were calculated based on STAR.log files using a
584 customised python script (available online via
585 https://github.com/hschilbert/3xODD/blob/main/parse_STAR_log_file_create_mapping_statis
586 tic.py). We used featureCounts v2.0.1 (94) with the -O --fraction parameters to generate count
587 tables based on the *A. thaliana* araport11 gff3 file (95) in order to assign a fractional count of
588 1/y from a reads, where y is the total number of meta-features/features overlapping with the
589 reads.

590 **Analysis of differentially expressed genes**

591 To identify differentially expressed genes (DEGs) between Col-0, Nö-0 and the *f3h*/*fls1*/*ans*
592 mutant in young seedlings, DESeq2 (96) was used to identify DEGs with a $\log_2$ fold change >1
593 and adjusted p-value <0.05 were selected for downstream analysis. Selected DEGs (86 DEGs
594 derived from the comparison of *f3h*/*fls1*/*ans* mutant to both wildtypes) were manually curated
595 by in-depth analysis of DEG's RNA-Seq read coverage against the TAIR10 reference genome
596 sequence to exclude DEGs arising from mapping artefacts, e.g., genes with partial read
597 coverage. The Venn diagram was generated using
598 https://bioinformatics.psb.ugent.be/webtools/Venn/.

599 **Flavonoid staining in *A. thaliana***

600 Visualisation of DPBA/Triton X-100-stained flavonoids in norflurazon-bleached *A. thaliana*
601 seedlings was performed according to Stracke *et al.* (97) using epifluorescence microscopy.
602 Visualisation of flavonoids in ethanol-bleached siliques of adult *A. thaliana* plants was
603 performed according to Stracke *et al.* (98).

604 **High performance thin layer chromatography (HPTLC) of flavonols and**
605 **dihydroflavonols**

606 Plants for flavonols extraction were grown in a greenhouse with 16 h of light illumination per
607 day at 22 °C. Extraction and analysis of dihydroflavonol and flavonol glycoside compounds
608 were performed as described in Stracke *et al.* (49). Siliques were homogenised in 80 %
609 methanol, incubated at 70 °C for 15 min and centrifuged at 14,000 x g for 10 min. After
610 vacuum-drying of the resulting supernatants, the dried pellets were redissolved in 80 %
611 methanol and analysed by HPTLC on a Silica Gel 60 plate (Merck, Darmstadt, Germany). The
612 mobile phase used was ethyl acetate, formic acid, acetic acid and water (100:26:12:12).
613 Dihydroflavonols and flavonol glycosides were detected by DPBA staining and UV light.

614 **(Poly)phenol extraction and targeted Ultra Performance Liquid Chromatography**
615 **– Multiple Reaction Monitoring Mass Spectrometry (UPLC-MS/MS MRM) analysis**

616 Samples of plant material were taken directly in the laboratory, lyophilized, and stored at room
617 temperature until used for further analysis. 100 mg of ground tissue were mixed with 1 mL of
618 80 % methanol for extraction of (poly)phenolic compounds. Samples and solvent were mixed
619 on an orbital shaker for 1 h at room temperature, sonicated for 30 min and the extraction
620 continued overnight at 4 °C in the dark. Each extract was filtered through a MILLEX 13-0.22 µm
621 PTFE membrane into glass vials and analysed as follows.
622 Sample extracts were injected immediately after filtration. Targeted UPLC-MS/MS with MRM
623 quantification analysis was performed on a Waters Acquity UPLC system (Milford, MA, USA)
624 consisting of a binary pump, an online vacuum degasser, an autosampler and a column
625 compartment. Separation of the phenolic compounds was conducted on a Waters Acquity HSS
626 T3 column 1.8 µm, 100 mm × 2.1 mm, kept at 40 °C. The analysis of phenolic compounds was
627 performed according to the method described by Vrhovsek *et al.* (99) using water with 0.1 %
628 formic acid and acetonitrile with 0.1 % formic acid as mobile phases for the gradient.
629 Mass spectrometry detection was performed on a Waters Xevo TQMS instrument equipped
630 with an electrospray ionisation (ESI) source. The capillary voltage was 3.5 kV in positive mode
631 and −2.5 kV in negative mode; the source was maintained at 150 °C; the desolvation

632 temperature was 500 °C; cone gas flow was 50 L/h; and desolvation gas flow was 800 L/h.
633 Unit resolution was applied to each quadrupole. Prior to UPLC-MS/MS MRM analysis, infusion
634 of each individual standard was performed to optimize the MRM conditions for quantification.
635 Data processing was performed using the Mass Lynx TargetLynx Application Manager
636 (Waters).

637 **Ultra-Performance Liquid Chromatography - Traveling Wave Ion Mobility-Mass**
638 **Spectrometry - Quadrupole Time of Flight (UPLC-TWIMS-QToF) Mass**
639 **Spectrometry and tandem mass spectrometry (UPLC-MS/MS) analysis**

640 The metabolite profile of Col-0 and *f3h*/*fls1*/*ans* biological replicate sample extracts were
641 acquired in an UPLC Acquity I system (Waters Corporation) coupled to a high-resolution mass
642 spectrometer HDMS Synapt XS (Waters Corporation). The chromatographic methodology was
643 performed according to Arapitsas *et al.* (100) with some modifications. The chromatographic
644 separation was carried out in an Acquity Premier HSS T3 1.8 µm, 2.1 x 100 mm column
645 (Waters) at 40 °C. The mobile phases A and B consisted of water with 0.1 % of formic acid
646 and methanol with 0.1 % formic acid, respectively, pumped with a flow rate of 0.3 mL/min. High
647 definition MS^e ($HDMS^e$) data acquisition with a scan time of 0.2 s was performed in continuum
648 mode with a mass range of 50-2000 Da in resolution mode (≥ 21500 FWHM at *m/z* 785), for
649 both ionisation modes (ESI+ and ESI-). The source temperature was settled at 120 °C, the
650 desolvation temperature at 450 °C, the nebuliser gas volume flow was 50 L/h and the
651 desolvation gas volume flow rate was 800 L/h. For ESI- acquisition mode, the capillary voltage
652 was 2.0 kV, and sampling cone was 30 V, whereas for ESI+ mode, the capillary voltage was
653 3.0 kV, and the sampling cone was 40 V. A collision energy ramp of 20-40 V was applied in
654 the transfer cell for high energy. For the ion mobility separation, the helium cell flow rate was
655 180 mL/min and for nitrogen it was 90 mL/min. The wave velocity was set to 650 m/s and the
656 transfer wave velocity to 141 m/s. The calibration was performed using the Major Mix IMS/ToF
657 Calibration kit solution (Waters Corporation). A leucine enkephalin solution (200 pg/µL) was
658 continuously infused as lock mass at flow rate of 10 µL/min during the whole analysis.
659 MassLynx v.4.2 and UNIFI software (Waters Corporation) were used for data acquisition and

660 processing. The collision cross sections (CCS) obtained were compared with an *in-house*
661 standard library.
662 A target UPLC-MSMS analysis was performed with the same source conditions in resolution
663 mode in a range of 50-2000 Da, with a scan time of 1 s. The collision energy was applied as a
664 ramp in the trap from 10-50 V for ESI- and 10-40 V for ESI+.

665 **Determination of anthocyanin accumulation**

666 Anthocyanin accumulation was visualised in 6-days-old seedlings grown on filter paper soaked
667 with 3 ppm of the bleaching herbicide norflurazon supplemented with 4 % sucrose to induce
668 anthocyanin accumulation. In addition, anthocyanin content was quantified photometrically in
669 6-days-old seedlings grown on 0.5 MS plates with 4 % sucrose as described by Mehrtens *et*
670 *al.* (101). Three independent biological replicates were measured for each sample.
671

672 ## Declarations

673 **Ethics approval and consent to participate**

674 Not applicable.

675 **Consent for publication**

676 Not applicable.

677 **Availability of data and materials**

678 All sequence data generated in this study are available under the ENA/NCBI Bioproject ID
679 PRJEB60353. In detail, the RNA-Seq data of *A. thaliana* Col-0, Nö-0, and the *f3h*/*fls1*/*ans*
680 mutant can be found with under the ENA/NCBI IDs: ERS14716218 - ERS14716221,
681 ERS14716222 - ERS14716225 and ERS14716226 - ERS14716229, respectively. The
682 genomic ONT data can be accessed using the ENA/NCBI IDs: ERS14716230 (FASTQ) and
683 ERS14716231 (FAST5). The *A. thaliana f3h*/*fls1*/*ans* mutant ONT assembly can be accessed
684 at the DOI: 10.4119/unibi/2979807.

Cometing interests

The authors declare that they have no competing interest.

Funding

This research was funded by the BMBF project RaPEQ, grant numbers "FKZ 031B0888A" (RaPEQ-2) and "FKZ 031B1305B" (RaPEQ-3), as well as by core funding of the Chair of Genetics and Genomics of Plants provided by Bielefeld University through Faculty of Biology. We acknowledge support for the publication costs by the Open Access Publication Fund of Bielefeld University and the Deutsche Forschungsgemeinschaft (DFG).

Authors‘ contributions

MB, HMS, RS and BW conceived and designed the research. MB, HMS, RS and SM carried out experiments and analysed the data. VS performed high resolution mass spectrometry experiments and interpreted the data. AA performed the metabolite quantification methodology. RS and BW supervised the project. MB and HMS drafted the manuscript. RS, SM and BW revised the manuscript.

Acknowledgments

We thank Andrea Voigt, Melanie Kuhlmann and Nicoletta Schmidt for excellent technical assistance and Martin Sagasser for fruitful discussions. Moreover, we thank Nils Kleinbölting for his support regarding *loreta*. We thank the Center for Biotechnology (CeBiTec) at Bielefeld University for providing an environment to perform the computational analyses.

References

1. Wen W, Alseekh S, Fernie AR. Conservation and diversification of flavonoid metabolism in the plant kingdom. Current Opinion in Plant Biology. 2020;55:100-8.

2. Winkel-Shirley B. Flavonoid biosynthesis. A colorful model for genetics, biochemistry, cell biology, and biotechnology. Plant Physiology. 2001;126:485-93.

3. Ishikura N, Yoshitama K. Anthocyanin-Flavonol Co-pigmentation in Blue Seed Coats of Ophiopogon jaburan. Journal of Plant Physiology. 1984;115(2):171-5.

712 4. Gronquist M, Bezzerides A, Attygalle A, Meinwald J, Eisner M, Eisner T. Attractive and
713 defensive functions of the ultraviolet pigments of a flower *(Hypericum calycinum)*. Proceedings
714 of the National Academie of Sciences of the United States of America. 2001;98(24):13745-50.

715 5. Grotewold E. The Science of Flavonoids. Grotewold E, editor. Columbus, Ohio, USA:
716 Springer New York, NY; 2006. 274 p.

717 6. Peer WA, Murphy AS. Flavonoids and auxin transport: modulators or regulators?
718 Trends in Plant Science. 2007;12(12):556-63.

719 7. Mo Y, Nagel C, Taylor LP. Biochemical complementation of chalcone synthase mutants
720 defines a role for flavonols in functional pollen. Proceedings of the National Academy of
721 Sciences of the United States of America. 1992;89:7213-7.

722 8. Li J, Ou-Lee TM, Raba R, Amundson RG, Last RL. Arabidopsis Flavonoid Mutants Are
723 Hypersensitive to UV-B Irradiation. The Plant Cell. 1993;5(2):171-9.

724 9. Xie P, Shi JY, Tang SY, Chen CX, Khan A, Zhang FX, et al. Control of Bird Feeding
725 Behavior by Tannin1 through Modulating the Biosynthesis of Polyphenols and Fatty Acid-
726 Derived Volatiles in Sorghum. Molecular Plant. 2019;12(10):1315-24.

727 10. Dauer A, Hensel A, Lhoste E, Knasmüller S, Mersch-Sundermann V. Genotoxic and
728 antigenotoxic effects of catechin and tannins from the bark of Hamamelis virginiana L. in
729 metabolically competent, human hepatoma cells (Hep G2) using single cell gel
730 electrophoresis. Phytochemistry. 2003;63(2):199-207.

731 11. Kandil FE, Smith MA, Rogers RB, Pepin MF, Song LL, Pezzuto JM, et al. Composition
732 of a chemopreventive proanthocyanidin-rich fraction from cranberry fruits responsible for the
733 inhibition of 12-O-tetradecanoyl phorbol-13-acetate (TPA)-induced ornithine decarboxylase
734 (ODC) activity. Journal of Agricultural and Food Chemistry. 2002;50(5):1063-9.

735 12. Schijlen E, Ric de Vos CH, Jonker H, van den Broeck H, Molthoff J, van Tunen A, et al.
736 Pathway engineering for healthy phytochemicals leading to the production of novel flavonoids
737 in tomato fruit. Plant Biotechnology Journal. 2006;4(4):433-44.

738 13. Reddy AM, Reddy VS, Scheffler BE, Wienand U, Reddy AR. Novel transgenic rice
739 overexpressing anthocyanidin synthase accumulates a mixture of flavonoids leading to an
740 increased antioxidant potential. Metabolic Engineering. 2007;9(1):95-111.

741 14. Scharbert S, Hofmann T. Molecular definition of black tea taste by means of quantitative
742 studies, taste reconstitution, and omission experiments. Journal of Agricultural and Food
743 Chemistry. 2005;53(13):5377-84.

744 15. Koornneef M. Mutations affecting the testa colour in Arabidopsis. Arabidopsis
745 Information Services. 1990;27:1-4.

746 16. Ito T, Motohashi R, Kuromori T, Mizukado S, Sakurai T, Kanahara H, et al. A new
747 resource of locally transposed Dissociation elements for screening gene-knockout lines in
748 silico on the Arabidopsis genome. Plant Physiology. 2002;129(4):1695-9.

749 17. Rosso MG, Li Y, Strizhov N, Reiss B, Dekker K, Weisshaar B. An *Arabidopsis thaliana*
750 T-DNA mutagenised population (GABI-Kat) for flanking sequence tag based reverse genetics.
751 Plant Molecular Biology. 2003;53(1-2):247-59.

752 18. Alonso JM, Stepanova AN, Leisse TJ, Kim CJ, Chen H, Shinn P, et al. Genome-wide
753 insertional mutagenesis of Arabidopsis thaliana. Science. 2003;301(5633):653-7.

754 19. Ferrer J-L, Jez JN, Bowman ME, Dixon RA, Noel JP. Structure of chalcone synthase
755 and the molecular basis of plant polyketide biosynthesis. Nature Structural Biology.
756 1999;6(8):775-84.

757 20. Jez JM, Bowman ME, Dixon RA, Noel JP. Structure and mechanism of the
758 evolutionarily unique plant enzyme chalcone isomerase. Nature Structural Biology.
759 2000;7(9):786-91.

760 21. Owens DK, Crosby KC, Runac J, Howard BA, Winkel BS. Biochemical and genetic
761 characterization of Arabidopsis flavanone 3beta-hydroxylase. Plant Physiology and
762 Biochemistry. 2008;46(10):833-43.

763 22. Schoenbohm C, Martens S, Eder C, Forkmann G, Weisshaar B. Identification of the
764 *Arabidopsis thaliana* flavonoid 3'-hydroxylase gene and functional expression of the encoded
765 P450 enzyme. Biological Chemistry. 2000;381:749-53.

766 23. Martens S, Forkmann G. Cloning and expression of flavone synthase II from Gerbera
767 hybrids. The Plant Journal. 1999;20(5):611-8.

768 24. Gebhardt YH, Witte S, Steuber H, Matern U, Martens S. Evolution of flavone synthase
769 I from parsley flavanone 3beta-hydroxylase by site-directed mutagenesis. Plant Physiology.
770 2007;144(3):1442-54.

771 25. Ali MB, McNear DHJ. Induced transcriptional profiling of phenylpropanoid pathway
772 genes increased flavonoid and lignin content in Arabidopsis leaves in response to microbial
773 products. BMC Plant Biology. 2014;14(84).

774 26. Falcone Ferreyra ML, Emiliani J, Rodriguez EJ, Campos-Bermudez VA, Grotewold E,
775 Casati P. The Identification of Maize and Arabidopsis Type I FLAVONE SYNTHASEs Links
776 Flavones with Hormones and Biotic Interactions. Plant Physiology. 2015;169(2):1090-107.

777 27. Owens DK, Alerding AB, Crosby KC, Bandara AB, Westwood JH, Winkel BS.
778 Functional analysis of a predicted flavonol synthase gene family in Arabidopsis. Plant
779 Physiology. 2008;147(3):1046-61.

780 28. Shirley BW, Hanley S, Goodman HM. Effects of ionizing radiation on a plant genome:
781 analysis of two Arabidopsis transparent testa mutations. The Plant Cell. 1992;4:333-47.

782 29. Davies KM, Schwinn KE, Deroles SC, Manson DG, Lewis DH, Bloor SJ, et al.
783 Enhancing anthocyanin production by altering competition for substrate between flavonol
784 synthase and dihydroflavonol 4-reductase. Euphytica. 2003;131(3):259-68.

785 30. Wilmouth RC, Turnbull JJ, Welford RW, Clifton IJ, Prescott AG, Schofield CJ. Structure
786 and mechanism of anthocyanidin synthase from *Arabidopsis thaliana*. Structure.
787 2002;10(1):93-103.

788 31. Xie DY, Sharma SB, Paiva NL, Ferreira D, Dixon RA. Role of anthocyanidin reductase,
789 encoded by BANYULS in plant flavonoid biosynthesis. Science. 2003;299(5605):396-9.

790 32. Zhang Y, Butelli E, Martin C. Engineering anthocyanin biosynthesis in plants. Current
791 Opnion in Plant Biology. 2014;19:81-90.

792 33. Tohge T, Nishiyama Y, Hirai MY, Yano M, Nakajima J, Awazuhara M, et al. Functional
793 genomics by integrated analysis of metabolome and transcriptome of Arabidopsis plants over-
794 expressing an MYB transcription factor. The Plant Journal. 2005;42(2):218-35.

795 34. Jones P, Messner B, Nakajima J, Schaffner AR, Saito K. UGT73C6 and UGT78D1,
796 glycosyltransferases involved in flavonol glycoside biosynthesis in *Arabidopsis thaliana*.
797 Journal of Biological Chemistry. 2003;278(45):43910-8.

798 35. Kim JH, Kim BG, Park Y, Ko JH, Lim CE, Lim J, et al. Characterization of flavonoid 7-
799 O-glucosyltransferase from Arabidopsis thaliana. Bioscience, Biotechnology, and
800 Biochemistry. 2006;70(6):1471-7.

801 36. Cheng AX, Han XJ, Wu YF, Lou HX. The function and catalysis of 2-oxoglutarate-
802 dependent oxygenases involved in plant flavonoid biosynthesis. International Journal of
803 Molecular Sciences. 2014;15(1):1080-95.

804 37. Kawai Y, Ono E, Mizutani M. Evolution and diversity of the 2-oxoglutarate-dependent
805 dioxygenase superfamily in plants. The Plant Journal. 2014;78(2):328-43.

806 38. Prescott AG, Lloyd MD. The iron(II) and 2-oxoacid-dependent dioxygenases and their
807 role in metabolism. Natural Product Reports. 2000;17(4):367-83.

808 39. Trewick SC, Henshaw TF, Hausinger RP, Lindahl T, Sedgwick B. Oxidative
809 demethylation by Escherichia coli AlkB directly reverts DNA base damage. Nature.
810 2002;419(6903):174-8.

811 40. Turnbull JJ, Nakajima J, Welford RW, Yamazaki M, Saito K, Schofield CJ. Mechanistic
812 studies on three 2-oxoglutarate-dependent oxygenases of flavonoid biosynthesis:
813 anthocyanidin synthase, flavonol synthase, and flavanone 3-beta-hydroxylase. Journal of
814 Biological Chemistry. 2004;279(2):1206-16.

815 41. Martens S, Preuß A, Matern U. Multifunctional flavonoid dioxygenases: Flavonol and
816 anthocyanin biosynthesis in Arabidopsis thaliana L. Phytochemistry. 2010;71(10):1040-9.

817 42. Busche M, Acatay C, Martens S, Weisshaar B, Stracke R. Functional Characterisation
818 of Banana (Musa spp.) 2-Oxoglutarate-Dependent Dioxygenases Involved in Flavonoid
819 Biosynthesis. Frontiers in Plant Science. 2021;12:701780.

820 43. Turnbull JT, Sobey WJ, Aplin RT, Hassan A, Firmin JL, Schofield CJ, et al. Are
821 anthocyanidins the immediate products of anthocyanidin synthase? Chemical
822 Communications. 2000:2473-4.

823 44. Yan Y, Chemler J, Huang L, Martens S, Koffas MA. Metabolic engineering of
824 anthocyanin biosynthesis in Escherichia coli. Applied and Environmental Microbiology.
825 2005;71(7):3617-23.

826 45. Park S, Kim DH, Park BR, Lee JY, Lim SH. Molecular and Functional Characterization
827 of Oryza sativa Flavonol Synthase (OsFLS), a Bifunctional Dioxygenase. Journal of
828 Agricultural and Food Chemistry. 2019;67(26):7399-409.

829 46. Schilbert HM, Schöne M, Baier T, Busche M, Viehöver P, Weisshaar B, et al.
830 Characterization of the *Brassica napus* flavonol synthase gene family reveals bifunctional
831 flavonol synthases. Frontiers in Plant Science. 2021;12:733762.

832 47. Yonekura-Sakakibara K, Higashi Y, Nakabayashi R. The Origin and Evolution of Plant
833 Flavonoid Metabolism. Frontiers in Plant Science. 2019;10:943.

834 48. Prescott AG, Stamford NPJ, Wheeler G, Firmin JL. In vitro properties of a recombinant
835 flavonol synthase from *Arabidopsis thaliana*. Phytochemistry. 2002;60(6):589-93.

49. Stracke R, De Vos RCH, Bartelniewoehner L, Ishihara H, Sagasser M, Martens S, et al. Metabolomic and genetic analyses of flavonol synthesis in *Arabidopsis thaliana* support the *in vivo* involvement of leucoanthocyanidin dioxygenase. Planta. 2009;229(2):427-45.

50. Wisman E, Hartmann U, Sagasser M, Baumann E, Palme K, Hahlbrock K, et al. Knock-out mutants from an En-1 mutagenized *Arabidopsis thaliana* population generate new phenylpropanoid biosynthesis phenotypes. Proceedings of the National Academy of Sciences of the United States of America. 1998;95(21):12432-7.

51. Abrahams S, Lee E, Walker AR, Tanner GJ, Larkin PJ, Ashton AR. The Arabidopsis TDS4 gene encodes leucoanthocyanidin dioxygenase (LDOX) and is essential for proanthocyanidin synthesis and vacuole development. The Plant Journal. 2003;35(5):624-36.

52. Bowerman PA, Ramirez MV, Price MB, Helm RF, Winkel BS. Analysis of T-DNA alleles of flavonoid biosynthesis genes in Arabidopsis ecotype Columbia. BMC Research Notes. 2012;5.

53. Routaboul JM, Kerhoas L, Debeaujon I, Pourcel L, Caboche M, Einhorn J, et al. Flavonoid diversity and biosynthesis in seed of *Arabidopsis thaliana*. Planta. 2006;224(1):96-107

54. Pelletier MK, Burbulis IE, Shirley BW. Disruption of specific flavonoid genes enhances the accumulation of flavonoid enzymes and endproducts in Arabidopsis seedlings. Plant Molecular Biology. 1999;40(1):45-54.

55. Appelhagen I, Thiedig K, Nordholt N, Schmidt N, Huep G, Sagasser M, et al. Update on *transparent testa* mutants from *Arabidopsis thaliana*: characterisation of new alleles from an isogenic collection. Planta. 2014;240(5):955-70.

56. Jupe F, Rivkin AC, Michael TP, Zander M, Motley ST, Sandoval JP, et al. The complex architecture and epigenomic impact of plant T-DNA insertions. PLoS Genetics. 2019;15(1):e1007819.

57. Pucker B, Kleinbolting N, Weisshaar B. Large scale genomic rearrangements in selected Arabidopsis thaliana T-DNA lines are caused by T-DNA insertion mutagenesis. BMC Genomics. 2021;22(1):599.

58. Rajapriya V, Kannan P, Sridevi G, Veluthambi K. A rare transgenic event of rice with Agrobacterium binary vector backbone integration at the right T-DNA border junction. J Plant Biochem Biot. 2021;30(3):421-8.

59. Wu H, Sparks CA, Jones HD. Characterisation of T-DNA loci and vector backbone sequences in transgenic wheat produced by Agrobacterium-mediated transformation. Molecular Breeding. 2006;18(3):195-208.

60. Monte E, Alonso JM, Ecker JR, Zhang YL, Li X, Young J, et al. Isolation and characterization of phyC mutants in Arabidopsis reveals complex crosstalk between phytochrome signaling pathways. The Plant Cell. 2003;15(9):1962-80.

61. Gao J, Peng H, Chen FB, Luo M, Li WB. Genome-wide analysis of transcription factors related to anthocyanin biosynthesis in carmine radish (Raphanus sativus L.) fleshy roots. PeerJ. 2019;7:e8041.

62. Reinhardt N. Untersuchung der katalytischen Eigenschaften Tropinonreduktase-ähnlicher kurzkettiger Dehydrogenasen/Reduktasen aus Brassicaceen. Halle (Saale): Martin-Luther-Universität Halle-Wittenberg; 2014.

879 63. Xu Z, Escamilla-Trevino L, Zeng L, Lalgondar M, Bevan D, Winkel B, et al. Functional
880 genomic analysis of *Arabidopsis thaliana* glycoside hydrolase family 1. Plant Molecular
881 Biology. 2004;55(3):343-67.

882 64. Ishihara H, Tohge T, Viehöver P, Fernie AR, Weisshaar B, Stracke R. Natural variation
883 in flavonol accumulation in Arabidopsis is determined by the flavonol glucosyltransferase
884 BGLU6. Journal of Experimental Botany. 2016;67(5):1505-17.

885 65. Miyahara T, Sakiyama R, Ozeki Y, Sasaki N. Acyl-glucose-dependent
886 glucosyltransferase catalyzes the final step of anthocyanin formation in Arabidopsis. Journal
887 of Plant Physiology. 2013;170(6):619-24.

888 66. Sugiyama R, Li R, Kuwahara A, Nakabayashi R, Sotta N, Mori T, et al. Retrograde
889 sulfur flow from glucosinolates to cysteine in Arabidopsis thaliana. Proceedings of the National
890 Academy of Sciences of the United States of America. 2021;118(22):e2017890118.

891 67. Duggleby RG, McCourt JA, Guddat LW. Structure and mechanism of inhibition of plant
892 acetohydroxyacid synthase. Plant Physiology and Biochemistry. 2008;46(3):309-24.

893 68. Turnbull JJ, Nagle MJ, Seibel JF, Welford RW, Grant GH, Schofield CJ. The C-4
894 stereochemistry of leucocyanidin substrates for anthocyanidin synthase affects product
895 selectivity. Bioorganic & Medicinal Chemistry Letters. 2003;13(21):3853-7.

896 69. Welford RWD, Turnbull JJ, Claridge TDW, Prescott AG, Schofield CJ. Evidence for
897 oxidation at C-3 of the flavonoid C-ring during anthocyanin biosynthesis. Chemical
898 Communications. 2001(18):1828-9.

899 70. Preuss A, Stracke R, Weisshaar B, Hillebrecht A, Matern U, Martens S. *Arabidopsis*
900 *thaliana* expresses a second functional flavonol synthase. FEBS Letters. 2009;583(12):1981–
901 6.

902 71. Li DD, Ni R, Wang PP, Zhang XS, Wang PY, Zhu TT, et al. Molecular Basis for
903 Chemical Evolution of Flavones to Flavonols and Anthocyanins in Land Plants. Plant
904 Physiology. 2020;184(4):1731-43.

905 72. Pucker B, Iorizzo M. Apiaceae FNS I originated from F3H through tandem gene
906 duplication. PLoS One. 2023;18(1):e0280155.

907 73. Han XJ, Wu YF, Gao S, Yu HN, Xu RX, Lou HX, et al. Functional characterization of a
908 *Plagiochasma appendiculatum* flavone synthase I showing flavanone 2-hydroxylase activity.
909 FEBS Letters. 2014;588(14):2307-14.

910 74. Lee YJ, Kim JH, Kim BG, Lim Y, Ahn JH. Characterization of flavone synthase I from
911 rice. BMB Reports. 2008;41(1):68-71.

912 75. Wang Y, Shi Y, Li K, Yang D, Liu N, Zhang L, et al. Roles of the 2-Oxoglutarate-
913 Dependent Dioxygenase Superfamily in the Flavonoid Pathway: A Review of the Functional
914 Diversity of F3H, FNS I, FLS, and LDOX/ANS. Molecules. 2021;26(21):6745.

915 76. Lukacin R, Wellmann F, Britsch L, Martens S, Matern U. Flavonol synthase from *Citrus*
916 *unshiu* is a bifunctional dioxygenase. Phytochemistry. 2003;62(3):287-92.

917 77. Zhang JR, Trossat-Magnin C, Bathany K, Negroni L, Delrot S, Chaudiere J. Oxidative
918 Transformation of Dihydroflavonols and Flavan-3-ols by Anthocyanidin Synthase from Vitis
919 vinifera. Molecules. 2022;27(3):1047.

920 78. Sheahan JJ, Cheong H, Rechnitz GA. The colorless flavonoids of *Arabidopsis thaliana*
921 (Brassicaceae). I. A model system to study the orthodihydroxy structure. American Journal of
922 Botany. 1998;85(4):467-75.

923 79. Reinhardt N, Fischer J, Coppi R, Blum E, Brandt W, Drager B. Substrate flexibility and
924 reaction specificity of tropinone reductase-like short-chain dehydrogenases. Bioorganic
925 Chemistry. 2014;53:37-49.

926 80. Xu F, Li L, Zhang W, Cheng H, Sun N, Cheng S, et al. Isolation, characterization, and
927 function analysis of a flavonol synthase gene from Ginkgo biloba. Molecular Biology Reports.
928 2012;39(3):2285-96.

929 81. Ley JP, Krammer G, Reinders G, Gatfield IL, Bertram HJ. Evaluation of bitter masking
930 flavanones from Herba Santa (Eriodictyon californicum (H. and A.) Torr., Hydrophyllaceae).
931 Journal of Agricultural and Food Chemistry. 2005;53(15):6061-6.

932 82. Buer CS, Sukumar P, Muday GK. Ethylene modulates flavonoid accumulation and
933 gravitropic responses in roots of Arabidopsis. Plant Physiology. 2006;140(4):1384-96.

934 83. Koren S, Walenz BP, Berlin K, Miller JR, Bergman NH, Phillippy AM. Canu: scalable
935 and accurate long-read assembly via adaptive k-mer weighting and repeat separation.
936 Genome Research. 2017;27(5):722-36.

937 84. Siadjeu C, Pucker B, Viehöver P, Albach DC, Weisshaar B. High Contiguity De Novo
938 Genome Sequence Assembly of Trifoliate Yam (Dioscorea dumetorum) Using Long Read
939 Sequencing. Genes. 2020;11(3):E274.

940 85. Simão FA, Waterhouse RM, Ioannidis P, Kriventseva EV, Zdobnov EM. BUSCO:
941 assessing genome assembly and annotation completeness with single-copy orthologs.
942 Bioinformatics. 2015;31(19):3210-2.

943 86. Lamesch P, Berardini TZ, Li D, Swarbreck D, Wilks C, Sasidharan R, et al. The
944 Arabidopsis Information Resource (TAIR): improved gene annotation and new tools. Nucleic
945 Acids Research. 2012;40(Database issue):D1202-D10.

946 87. Li H. Minimap2: pairwise alignment for nucleotide sequences. Bioinformatics.
947 2018;34(18):3094-100.

948 88. Li H, Handsaker B, Wysoker A, Fennell T, Ruan J, Homer N, et al. The Sequence
949 Alignment/Map format and SAMtools. Bioinformatics. 2009;25(16):2078-9.

950 89. Robinson JT, Thorvaldsdottir H, Winckler W, Guttman M, Lander ES, Getz G, et al.
951 Integrative genomics viewer. Nature Biotechnology. 2011;29(1):24-6.

952 90. Altschul SF, Gish W, Miller W, Myers EW, Lipman DJ. Basic local alignment search
953 tool. Journal of Molecular Biology. 1990;215(3):403-10.

954 91. Andrews S. FastQC, a quality control tool for high throughput sequence data. 2018
955 Available from: http://www.bioinformatics.babraham.ac.uk/projects/fastqc/

956 92. Lee H, Chawla HS, Obermeier C, Dreyer F, Abbadi A, Snowdon R. Chromosome-Scale
957 Assembly of Winter Oilseed Rape *Brassica napus*. Frontiers in Plant Science. 2020;11:496.

958 93. Dobin A, Davis CA, Schlesinger F, Drenkow J, Zaleski C, Jha S, et al. STAR: ultrafast
959 universal RNA-seq aligner. Bioinformatics. 2013;29(1):15-21.

960 94. Liao Y, Smyth GK, Shi W. featureCounts: an efficient general purpose program for
961 assigning sequence reads to genomic features. Bioinformatics. 2014;30(7):923-30.

962 95. Cheng CY, Krishnakumar V, Chan A, Thibaud-Nissen F, Schobel S, Town CD.
963 Araport11: a complete reannotation of the Arabidopsis thaliana reference genome. The Plant
964 Journal. 2017;89(4):789-804.

965 96. Love MI, Huber W, Anders S. Moderated estimation of fold change and dispersion for
966 RNA-seq data with DESeq2. Genome Biology. 2014;15(12):550.

967 97. Stracke R, Ishihara H, Huep G, Barsch A, Mehrtens F, Niehaus K, et al. Differential
968 regulation of closely related R2R3-MYB transcription factors controls flavonol accumulation in
969 different parts of the *Arabidopsis thaliana* seedling. The Plant Journal. 2007;50(4):660-77.

970 98. Stracke R, Jahns O, Keck M, Tohge T, Niehaus K, Fernie AR, et al. Analysis of
971 PRODUCTION OF FLAVONOL GLYCOSIDES-dependent flavonol glycoside accumulation in
972 *Arabidopsis thaliana* plants reveals MYB11-, MYB12- and MYB111-independent flavonol
973 glycoside accumulation. New Phytologist. 2010;188(4):985-1000.

974 99. Vrhovsek U, Masuero D, Gasperotti M, Franceschi P, Caputi L, Viola R, et al. A versatile
975 targeted metabolomics method for the rapid quantification of multiple classes of phenolics in
976 fruits and beverages. Journal of Agricultural and Food Chemistry. 2012;60(36):8831-40.

977 100. Arapitsas P, Mattivi F. LC-MS Untargeted Protocol for the Analysis of Wine. Methods
978 in Molecular Biology. 2018;1738:225-35.

979 101. Mehrtens F, Kranz H, Bednarek P, Weisshaar B. The Arabidopsis transcription factor
980 MYB12 is a flavonol-specific regulator of phenylpropanoid biosynthesis. Plant Physiology.
981 2005;138(2):1083-96.
982